

## Measurement of the $K_L^0$ Mean Life\*

Kirby G. Vosburgh,<sup>†</sup> Thomas J. Devlin, Robert J. Esterling,<sup>‡</sup>  
Barton Goz,<sup>§</sup> and Douglas A. Bryman<sup>||</sup>

*Physics Department, Rutgers—The State University, New Brunswick, New Jersey 08903*

and

W. E. Cleland\*\*

*Physics Department, University of Massachusetts, Amherst, Massachusetts 01002*

(Received 10 March 1972)

A new measurement of the mean life of the  $K_L^0$  meson was made in a scintillation-counter experiment by observing the exponential decrease in  $K_L^0$  flux as a function of distance in a collimated neutral beam. We find  $\tau = (5.154 \pm 0.044) \times 10^{-8}$  sec. This result strengthens the conclusion that the predictions of a pure  $\Delta I = \frac{1}{2}$  rule are not correct for  $K_{\pi_3}$  decay.

### I. INTRODUCTION

We have measured the mean life ( $\tau$ ) of the long-lived neutral  $K$  meson ( $K_L^0$ ) to be  $(5.154 \pm 0.044) \times 10^{-8}$  sec.<sup>1</sup> Two reasons motivated the experiment. First, we wished to obtain a more precise value for this fundamental property of one of the more interesting elementary particles. Second, we hoped to improve the validity of tests of the  $\Delta I = \frac{1}{2}$  rule in  $K_{\pi_3}$  decay.<sup>2-9</sup>

The  $\Delta I = \frac{1}{2}$  selection rule predicts several relations among the decay rates of  $K$  mesons into 3-pion final states. In particular, we have (among the ratios tabulated in Ref. 6)

$$T_3 = \frac{1}{2} [\Gamma(K^+ \rightarrow \pi^+ \pi^+ \pi^-) / \phi_3] [\Gamma(K_L^0 \rightarrow \pi^+ \pi^- \pi^0) / \phi_2]^{-1}. \quad (1)$$

Here  $\phi_3$  and  $\phi_2$  are correction factors which account for the available phase-space volume,<sup>2,7</sup> the final-state Coulomb interactions,<sup>2-9</sup> and the energy dependence of the transition amplitude.<sup>8,9</sup> Among the  $\Delta I = \frac{1}{2}$ -rule predictions,  $T_3$  is particularly sensitive to  $\Delta I = \frac{3}{2}$  contributions to the decay amplitudes. The previous experimental value<sup>6</sup> of  $T_3 = 1.22 \pm 0.05$  indicated a violation of the predictions of the rule. The presence of a  $\Delta I = \frac{3}{2}$  amplitude with 5% of the strength of the  $\Delta I = \frac{1}{2}$  term would explain the result. This is consistent with the magnitude of the 2-pion transition  $K^+ \rightarrow \pi^+ \pi^0$ , a process forbidden by the rule.

The ratio  $T_3$  is a comparison between a  $K^+$  partial rate and a  $K_L^0$  partial rate. The  $K^+$  measurements are sufficiently accurate that they contribute little to the uncertainty in  $T_3$ . Further, sufficient cross checks exist in the constrained fits to the data (total rates, partial rates, and branching ratios) that one can use the values with some confidence. The situation is different with  $K_L^0$  decays. Few direct measurements of partial rates exist,

and the lifetime measurements are the only direct precise measurements of absolute rates. The constrained fit provides little defense against a systematic error in  $\tau$ . We note that  $T_3$  is directly proportional to  $\tau$  and that approximately half of the uncertainty in  $T_3$  is due to the uncertainty in previous measurements of  $\tau$ .<sup>10-16</sup>

In the present experiment we extended and modified the technique used by Sayer *et al.*<sup>10,11</sup> We observed the exponential decrease in  $K_L^0$  rate as a function of distance and particle momentum in a collimated neutral beam. The careful control of systematic uncertainties in the present experiment draws heavily on the experience gained in the earlier work.

Details of the experimental setup are discussed in Sec. II. We present the data analysis in Sec. III, the results in Sec. IV, and discussion and conclusions in Sec. V.

### II. EXPERIMENTAL DETAILS

The rate of  $K_L^0$  decays counted by a detector is a function of its distance,  $D$ , from the kaon source, as follows:

$$N(D, P) = N_0(P) \epsilon(D, P) \Omega(D) \exp(-MD/P\tau), \quad (2)$$

where  $P$  is the momentum and  $M$  is the mass of the  $K_L^0$ ,  $N_0(P)$  is the production intensity,  $\Omega(D)$  is the solid angle subtended by the detector, and  $\epsilon(D, P)$  is the efficiency of the detector.  $N(D, P)$  is a rate measured by our detector, appropriately binned, normalized, and corrected for backgrounds. The distance  $D$  was measured to an accuracy far better than required. The solid angle was computed from geometry and checked by direct measurements. The ratio  $M/P$  was determined directly from time-of-flight measurements. (Thus, our results are independent of the assumed mass of the neutral

kaon.) The relative efficiency of the detector was calculated using Monte Carlo techniques. It is not necessary to know the absolute detection efficiency, since we need only the relative kaon rate at different positions.

#### A. Characteristics of the Beam

The experiment was performed at the Princeton-Pennsylvania Accelerator (PPA), where the  $K_L^0$  beam was created at  $90^\circ$  with respect to the 3-GeV internal proton beam incident on a Pt target. A floor plan of the beam is shown in Fig. 1.

The first 15 ft of the beam line were devoted to rough collimation, sweeping magnets, and shielding, while the remainder was used for the collimator and detector assemblies. The detector and collimator were mounted on separate carts so that they could be moved independently along 99 ft of rails parallel to the beam line. The detector cart could be moved 73 ft, corresponding to a range of 1.6–3.7 mean lives of the  $K_L^0$  in the momentum range detected.

Three sweeping magnets were used to remove charged particles from the beam, and a 2-in.-thick lead filter was placed in the beam near the synchrotron target to reduce the flux of  $\gamma$  rays. The beam line was evacuated to reduce the possibility of neutron interactions, which might simulate a decaying  $K_L^0$  meson. The vacuum line extended from the lead filter to a point 7 ft beyond the active volume of the detector.

The secondary beams of the PPA have a pronounced time structure caused by the tight bunching of the primary proton beam. This structure was used in determining the time of flight (TOF) of the neutral  $K$  mesons, as described in Sec. II E.

#### B. Collimators

The collimators produced a well-defined beam geometry in the  $K_L^0$  decay region. They are shown in Fig. 2. The primary collimator determined the solid-angle acceptance of the detection system [ $\Omega$  in Eq. (2)], while the secondary collimator stopped particles scattered in the primary collimator. A magnet with 250 kG in. of bending power was used to sweep out charged particles created in the collimator walls.

Since the efficiency of the  $K_L^0$  detector was slightly sensitive to variations of the transverse size of the beam in the decay region, the collimator position was changed to keep the beam size constant as the detector was moved to different positions along the beam line. Each time the collimator cart was moved, the collimators were aligned by sighting with a transit along the beam axis to a set of cross hairs located close to and centered on the synchrotron target. Both the front and rear ends of the primary collimator were adjusted so that their deviations from the surveyed beam line were less than 0.015 in. In general, the secondary collimator required no adjustment to stay within its required tolerance of 0.1 in.

The primary collimator was fitted with valves at each end so that the collimator could be closed off and filled with mercury. The collimator was filled after each data run for a measurement of backgrounds. This "mercury plug" was 5 ft thick and it filled the collimator completely. After each background run the collimator was drained, swabbed, and inspected to ensure that no mercury remained.

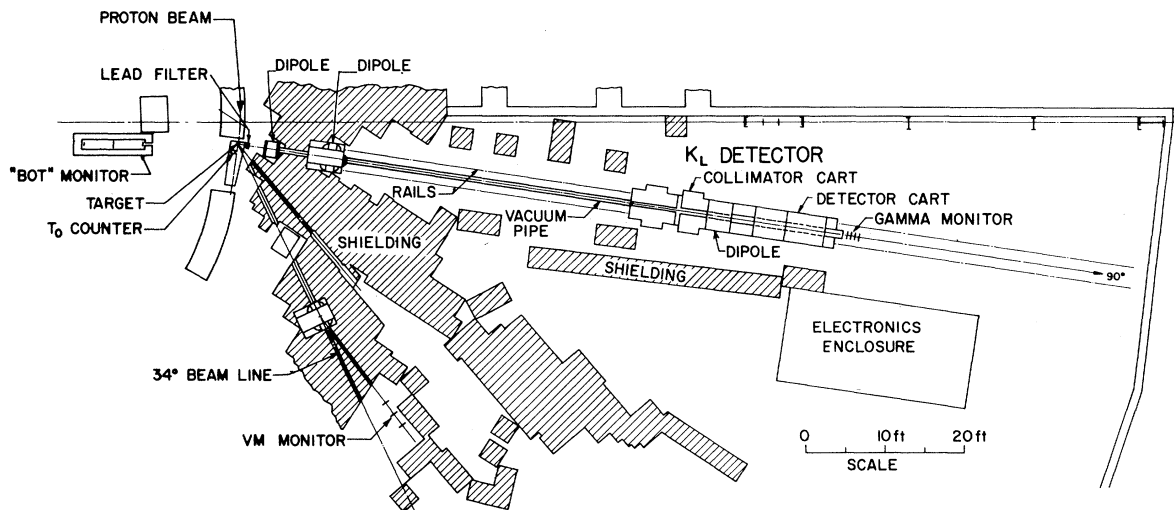


FIG. 1. Floor plan of the experimental area. The experiment was performed in the  $90^\circ$  neutral beam. Proton intensity monitors were placed in the  $34^\circ$  charged beam line, in the  $90^\circ$  neutral beam, and in the synchrotron room itself.

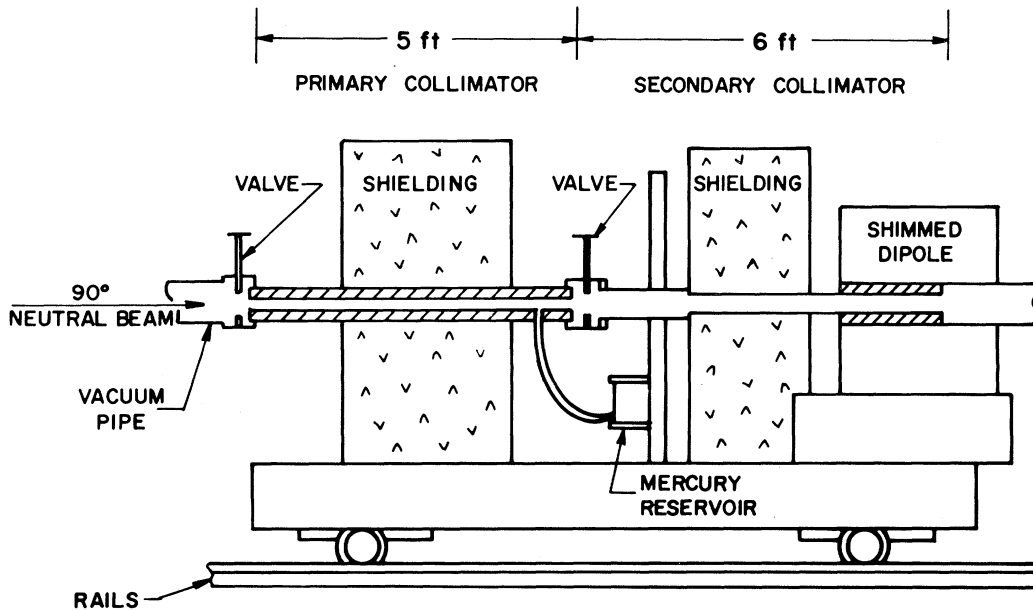


FIG. 2. Diagram of the collimation system consisting of a 5-ft-thick primary collimator with a 2½-in.-diameter aperture, a 6-ft-thick secondary collimator, a sweeping magnet, and various shielding blocks. The entire assembly weighed about 30 tons and was rolled from place to place along the beam line on railroad tracks by hitching a team of physicists to it.

### C. The $K_L^0$ Detection System

The  $K_L^0$  has four dominant decay modes:

- $K_L^0 \rightarrow \pi^+ \pi^- \pi^0$ ,  $12.6 \pm 0.6\%$
- $\rightarrow \pi^0 \pi^0 \pi^0$ ,  $21.5 \pm 0.9\%$
- $\rightarrow \pi^\pm e^\mp \bar{\nu}_e$ ,  $38.8 \pm 1.6\%$
- $\rightarrow \pi^\pm \mu^\mp \bar{\nu}_\mu$ ,  $26.8 \pm 1.2\%$ .

In addition, there are several rare decay modes, including the  $CP$ -violating  $K_L^0 \rightarrow 2\pi$  modes.

The  $K_L^0$  detector was designed on the same principle as that used by Sayer *et al.*<sup>11</sup>: In three of the four principal decay modes of the  $K_L^0$ , two charged particles are emitted, and it is these charged particles that are detected. The only other components of the beam, neutrons and  $\gamma$  rays, do not produce charged particles in a vacuum. (Neutron decays are  $10^{11}$  times more rare than kaon decays.) Electron-positron pairs from  $\gamma$ -ray interactions came at a fixed time in the TOF spectrum and thus could be recognized easily. The range requirements in the counter telescopes strongly suppressed the rare neutron-induced events from double scatters in the collimator walls.

The  $K_L^0$  detector consisted of four counter telescopes of equal length (4 ft parallel to the beam) but of different widths (see Fig. 3). The telescopes formed the sides of an asymmetric box, and the beam passed through the open ends.

Each telescope consisted of two ½-in.-thick plas-

### CROSS SECTION OF $K_L^0$ DETECTOR (LOOKING DOWNSTREAM)

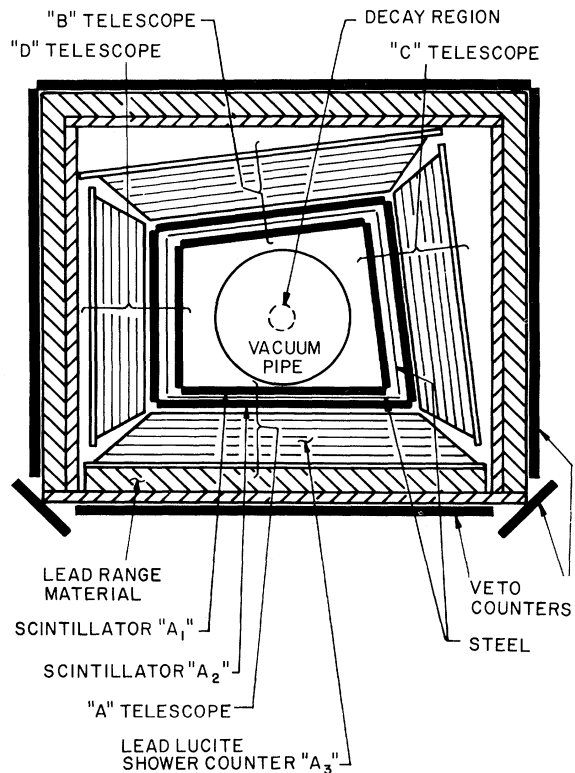


FIG. 3. Cross section of the  $K_L^0$  detector.

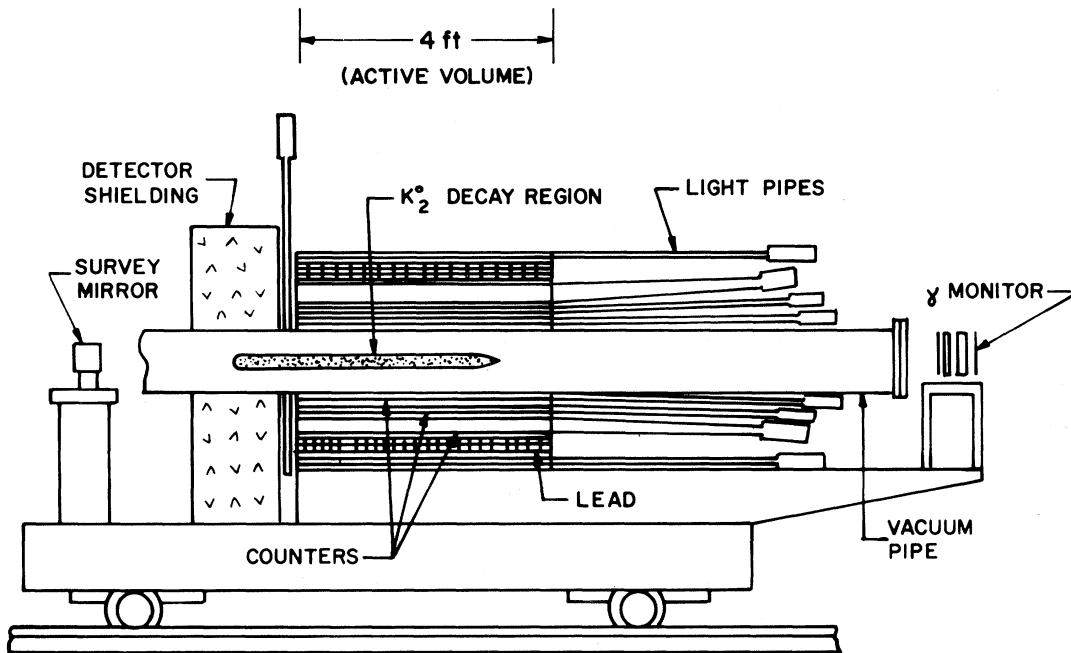


FIG. 4. Side view of the  $K_L^0$  detector cart. The light from the counters was collected at the downstream end by Lucite light pipes cut in adiabatic strips ending in 56AVP photomultipliers. The survey mirror was used in aligning the primary collimator.

tic scintillation counters separated by a  $\frac{1}{4}$ -in. steel plate, and then a lead-Lucite Čerenkov counter. The steel plate was inserted to act as a range requirement and to suppress accidental triggers from slow neutrons which filtered through the shielding. The lead-Lucite shower counter was used in an attempt to detect the  $3\pi^0$  decay mode and provided a sample of events particularly free from neutron background. The detector was surrounded by a 1-in.-thick layer of steel and a 2-in.-thick layer of lead to absorb the  $K_L^0$  decay products. It was covered as completely as possible by an array of cosmic-ray veto counters. The shielding was needed to keep the kaon decay products from triggering the veto counters.

The decay region for the  $K_L^0$  mesons extended from a point 2 ft upstream of the detector to the downstream end of the detector (see Fig. 4). In this region the vacuum-pipe diameter was 12 in. The pipe was made of  $\frac{1}{8}$ -in.-thick aluminum. The beam diameter was 3 in. full width at half maximum (FWHM). Horizontal profiles of the beam were made with a set of small scintillation counters, and the halo was found to be negligible ( $<0.5\%$  of the central flux density).

A telescope was considered to respond whenever a coincidence occurred between signals from the two inner scintillation counters. A response from two or more telescopes in the absence of any cosmic-ray veto counter pulse was the  $K_L^0$  decay sig-

nal. This signal, indicating that at least two charged particles came from the beam decay region, was used to determine the  $K_L^0$  TOF. It initiated a computer readout of the TOF and the pattern of counters that responded to the event.

Each of the counter signals was delayed 134 nsec (which is a multiple of the rf period of the proton beam) and again put into coincidence with the kaon trigger. This produced a continuous monitor of accidental triggers and accidental veto rates. Accidental triggers were less than 0.2% of the total event rate. The dead time due to pulses from the veto counters varied between 0.2 and 0.6%.

#### D. Monitors

Since the absolute flux of  $K_L^0$  mesons in our beam was not directly measurable, it was necessary to construct monitors to determine the relative flux. Each of the monitors was sensitive in a different way to the number of protons striking the production target. Our normalization procedure rests on the assumption that the  $K_L^0$  flux is proportional to the rates in these monitors for a given momentum of the primary proton beam. Other devices were used to monitor the live time of the electronics for cosmic-ray background corrections, and to monitor the solid angle subtended by our collimator system.

In addition to the obvious uses mentioned above,

these devices were used to perform a variety of other tasks related to calibrations, background measurements, stability checks. We shall describe each monitor, its characteristics, and its uses.

### 1. Beam-on-Target (BOT) Monitor

The BOT is a PPA facility consisting of three  $\frac{1}{4}$ -in. cubes of plastic scintillator, 3 ft apart, each viewed by two phototubes. The assembly is mounted inside the synchrotron room, pointed directly at the production target on a line at  $82^\circ$  relative to the proton beam (Fig. 1). It is surrounded by thick steel shielding with a small beam aperture.

### 2. VM Monitor

The VM monitor consisted of three 1-in.-diameter,  $\frac{1}{8}$ -in.-thick disks of plastic scintillator mounted 18 in. apart in a negatively charged beam (see Fig. 1). One of the photomultiplier signals was clipped and fed into a zero-cross discriminator to give precise timing information. The momentum of the negative beam was adjusted to the position of maximum intensity to avoid errors due to possible drifts in the magnet current. This also gave a transverse production momentum for pions of the same order as that in our kaon beam. The TOF measurements for these particles relative to the  $T_0$  counter (see Sec. II E) had a resolution of 1.2 nsec FWHM. The intensity of background counts coming at other times in its TOF spectrum was measured to be 0.1%.

The VM monitor served four functions: relative normalization of the  $K_L^0$  flux, monitoring of the efficiency of the TOF system, determination of intensity of primary protons in the "empty" phase-stable regions (see Sec. II E), and monitoring of the "dead time" of the detector due to spurious counts in the cosmic-ray veto counters.

### 3. GAMMA Monitor

The GAMMA monitor was constructed to be sensitive to  $\gamma$  rays and insensitive to charged particles and neutrons in the  $90^\circ$  beam. It consisted of two 8-in.-diameter scintillation counters and a water Čerenkov counter preceded by a charged-particle veto counter and a  $\frac{1}{8}$ -in.-thick piece of lead converter. It was mounted in the neutral beam at the rear of the  $K$  detector (see Fig. 1). The width of the TOF peak for  $\gamma$  rays was 1.2 nsec FWHM.

This monitor had several functions. It was used to check the relative normalization of different runs taken at the same position at widely separated times. It was used to monitor dead-time corrections for the cosmic-ray veto counters.

Since it held a fixed relationship to the  $K$  detector in position and timing, it was used to adjust the relative timing of the TOF system after each movement of the detector. This was done with the "time vernier" system described elsewhere.<sup>17</sup> Finally, it was used to determine one of the calibration constants ( $A_1$ ) of the TOF system, as described in Sec. II E.

### 4. Clock

The clock signal was derived from a crystal-controlled oscillator of high stability. The clock pulses had a frequency of 156.25 MHz. The clock was used to monitor the live time of the detector to enable corrections for the cosmic-ray backgrounds. This was necessary because the live time for our detection system was dependent on the conditions of the beam. The electronics were gated off during periods of low proton intensity to reduce the cosmic-ray background. Further, the rate of event triggers of the readout system caused fluctuations of the live time. The clock was also used to determine the efficiency of the TOF system for signals completely uncorrelated with the beam. This was found to be significantly different from that of beam-related signals. The results of this measurement were used in applying the cosmic-ray corrections (Sec. III B).

Because the energy of the protons striking the synchrotron target varied by 10% depending on the time in the spill (see Table I), the ratios of the rates of the monitors were functions of spill time. To alleviate this problem, we constructed a "correlator," a device which routed the monitor signals to different scalers as a function of the spill time. Each kaon decay was also tagged with its time in the spill, and the analysis for the mean lifetime was performed separately for each of the four correlator channels. Any inconsistency among these results produces a measure of the dependence of the final results on systematic effects due to

TABLE I. Characteristics of the spill correlator channels.

Spill correlator channel No.	Mean proton energy (GeV)	Correlator channel width (msec)	Proton bunch spacing <sup>a</sup> (nsec)
1	2.707	1.21	67.435
2	2.841	1.54	67.265
3	2.902	1.96	67.200
4	2.974	4.72	67.094

<sup>a</sup> These figures apply to the case of "single-chopped" injection. For "double-chopped" injection, they must be multiplied by 2.

changes in the rate and the incident proton energy. The parameters corresponding to each correlator channel are listed in Table I.

#### E. Time-of-Flight Measurements

The secondary beams of the PPA have a pronounced time structure. The bunches of protons striking the internal target of the synchrotron are small ( $\sim 1$  nsec) relative to their separation from one another ( $\sim 33$  nsec). This gives each secondary particle a well-defined creation time, modulo the proton bunch spacing, which, combined with the detection time of the particle, gives the TOF over a known distance. If the particle's identity (mass) is known, its momentum can be calculated. Further discussion and references to earlier TOF work may be found in the papers of Sayer *et al.*<sup>11</sup> and Shepard *et al.*<sup>17</sup> Because a 33-nsec period between proton bunches is short relative to most particle flight times encountered in our experiment, it was increased to 67 or 134 nsec in this experiment by "chopping" out alternate bunches (single-chopped) or 3 out of 4 bunches (double-chopped) in the eight phase-stable regions of the synchrotron. This was accomplished by electrostatic deflection of the low-energy beam before it was injected into the main ring of the synchrotron.

Because of the ambiguity in the creation time, the

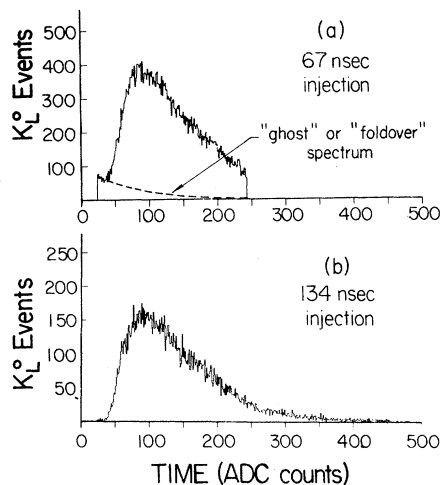


FIG. 5. The effect of small proton bunch spacing on a TOF spectrum. If a single bunch of protons were to hit the synchrotron target, without any other bunches preceding or following it, we would obtain a TOF spectrum like that shown in (b). If there is another bunch following the first at an interval of 67 nsec, the fast particles from the second bunch will catch up with the slow particles from the first, arriving at the detector at the same time as in (a). As far as TOF measurements are concerned, these sets of particles are indistinguishable.

TOF measured for a neutral particle is ambiguous. If the range of energies of the detected particles is large, this TOF ambiguity leads to a number of possible values for the particles' momentum. The spurious values give rise to the "ghost" or "fold-over" spectrum as shown in Fig. 5. This effect is important in this experiment since the lifetime of the  $K_L^0$ , as measured in the laboratory, is momentum-dependent. We have determined the magnitude of the ghost contamination by measuring spectra with proton bunch spacing large enough to reduce the ghost contamination to a negligible level. These data were included in the fit to the production spectrum parameters as described in Sec. III F.

The TOF system was used to measure the elapsed time between the creation of a  $K_L^0$  at the synchrotron target and its decay. The creation-time signal was obtained from a water Čerenkov counter located 2 ft from the synchrotron target. Known as  $T_0$ , this counter was similar to that used by Shepard *et al.*<sup>17</sup> The last four dynodes of the  $T_0$  photomultiplier were powered independently due to the high current drain. Two discriminators were used with  $T_0$ . Noise and small reflections were rejected by a leading-edge pulse-height discriminator, and the timing was determined by a zero-cross discriminator. The final  $T_0$  signal was sent through a precision variable delay and one of a set of fixed precision delays used to compensate for the position of the detector. The variable delay was adjusted until the time vernier came into balance (see below).

If a kaon-decay signal occurred, the  $T_0$  signal started a time-to-amplitude converter (TAC). The stop signal for the TAC was derived from the kaon signal during normal operation. The TAC output was sent to an analog-to-digital converter whose output was read by the on-line computer.

During auxiliary tests and calibrations other signals were used to stop the TAC. A pulser signal was used to test the linearity of the TOF system. Since the pulser signals are uncorrelated with the beam, the resulting time spectrum will be flat if the system is linear. Our spectra were flat to within the statistical accuracy of the tests, better than 1%. Other stop signals with well-defined timing (e.g., from the VM or GAMMA monitor) allowed us to measure the resolution of the TOF system, and typically peaks of 1.2 nsec FWHM were obtained in this way.

If an event was detected but the  $T_0$  signal from the proton bunch which created this event did not occur, a  $T_0$  pulse from one of the later bunches was used to determine the TOF. This procedure produces a series of spectra, each displaced by a multiple of the proton-bunch spacing. These dis-

placed spectra were shifted to coincide with the normal spectrum when analyzing the data, and the net result of the process was a gain in TOF efficiency. The displaced spectra contributed about 4% to a typical over-all efficiency of 98%. The TOF efficiency was monitored by scaling the coincidences between the VM monitor signal and  $T_0$  and comparing with the total number of VM counts.

The VM monitor was also used for monitoring alternate bucket contamination (ABC). ABC occurs when some of the proton bunches which are thought to be empty actually contain some beam due to inefficiency of the injection chopper. This was a serious contaminant, as it had the effect of mixing the momentum spectra (similar to ghost contamination). Since VM had a very well-defined TOF peak relative to  $T_0$ , any VM signal which occurred displaced from this peak by a multiple of 33 nsec was regarded as evidence that the injection chopper was not properly tuned. The displaced VM rate was monitored continuously and the ABC rate was generally kept at a level less than 0.1%. The chopper was retuned if the ABC rate exceeded this value.

Possible drifts in the  $T_0$  signal were monitored by the "time vernier" logic system.<sup>17</sup> It was sensitive to drifts of order 0.1 nsec. The time vernier was set up with the GAMMA-monitor signal so that relative timing of GAMMA and  $T_0$  could be monitored. Since the GAMMA monitor was mounted on the detector cart behind the kaon decay volume, its TOF peak was displaced by the same amount as the time origin of the kaon TOF spectrum. The variable delay in the  $T_0$  logic (as well as the large precision delay) was adjusted each time the cart was moved, until the time vernier reached a null state. This ensured that the TOF spectrum was always in the same operating range of the time-to-digital system. While this was not the method used to calibrate the TOF system, its results were in excellent agreement with the main calibration method.

Each time the detector was moved, the TOF system was calibrated. Assuming that the output of the TAC is a linear function of the time between the start and stop signals, two parameters are needed if the  $K_L^0$  momentum is to be determined from the TOF measurement: the zero offset and the scaling factor (nsec/channel). We define the time of "zero" to be that channel number which would be measured if the kaon were traveling at the speed of light, and call this  $A_0$ . In measuring the scaling factor, we define  $A_1$  as the number of channels corresponding to 67.17 (134.34) nsec, the rf period at a particular time in the spill of single-chopped (double-chopped) injection.

To measure  $A_0$  we placed a metal converter upstream of the detector and measured the time spec-

trum of electron-positron pairs from  $\gamma$ -ray interactions using the kaon detector. The peak of this spectrum, corrected as described in Sec. III B, is the measured value of  $A_0$ .

The value of  $A_1$  was determined by measuring the periodicity of the proton bunches using the GAMMA monitor. Because the energy of the protons, and hence the period of the bunches, changes during the spill (see Table I), we accepted signals from the monitor only during a 1-msec portion of the spill, for which the periodicity was known to be 67.17 or 134.34 nsec. The periodicity was observed by reducing the efficiency of the  $T_0$  logic system to a point where the time of flight was often determined by a later  $T_0$  pulse (see above). Since the spacing between the peaks in the TOF spectrum was equal to the known proton period, we measured  $A_1$  directly, finding  $A_1$  corresponding to  $3.25 \pm 0.01$  channels/nsec.

#### F. Operating Procedures

Data runs were taken with the kaon detector in six positions along the beam line (see Table II). At the positions further downstream, the synchrotron was run with double-chopped injection, so that the spacing between bursts of beam was 134 nsec. These conditions were necessary to minimize ghost ambiguity in determining the momentum at the downstream positions. We also took data with double-chopped injection at our farthest upstream position. Under these conditions, there were no ghosts and we obtained a complete spectrum down to the lowest momenta for use in analysis. Table II summarizes the different run types.

The detector was moved back and forth along the beam four times during the course of the data-taking, which covered about one month. This period followed several months of setting up and testing and approximately one month of preliminary running. Each run consisted of a set of three measurements: (1) a measurement of the relative  $K_L^0$  flux, (2) a measurement of the beam-related background and cosmic rays with the primary collimator filled with mercury to stop the direct beam, and (3) a measurement of the cosmic-ray background made with the logic system gated to exclude any beam from the synchrotron. In addition to the direct measurements of decay rates and backgrounds, the TOF system was calibrated before each run. In the final data set there are 25 sets of runs, divided about equally among the different run types.

The experiment was gated on over a 10-msec period for each cycle of the synchrotron. This time included all of the usable spill. The spill intensity was monitored, and when it was below a preset level the experiment was gated off. This

TABLE II. Characteristics of the data sets.

Run type	Nominal position (ft)	Detector center <sup>a</sup> (in.)	Collimator position <sup>a</sup> (in.)	Solid angle (msr)	Injection period (nsec)	Momentum range (MeV/c)	Raw events	Cosmic rays	Beam-related background
1	0	400.00	246.25	$6.837 \times 10^{-2}$	67	200–500	114 921	554	270
2	5	460.00	306.25	$4.387 \times 10^{-2}$	67	210–550	101 795	1057	434
3	15	580.00	426.25	$2.239 \times 10^{-2}$	67	250–600	79 977	2536	920
4	25	700.00	546.25	$1.357 \times 10^{-2}$	67	280–600	46 748	3528	1136
5	0	400.00	246.25	$6.837 \times 10^{-2}$	134	100–530	81 177	696	180
6	25	700.00	426.25	$2.239 \times 10^{-2}$	134	175–620	24 616	2112	351
7	50	1000.00	606.25	$9.088 \times 10^{-3}$	134	220–640	9553	2907	839
8	73	1274.75	810.25	$6.137 \times 10^{-3}$	134	250–660	17 741	8818	1362

<sup>a</sup> Distance measured from the synchrotron target.

process limited the “live time” to periods of “good beam,” thereby reducing the cosmic-ray background.

When a  $K_L^0$  event was detected, the fast electronics logic was immediately gated off. It was held off by various busy signals until the TOF analysis was complete and all data had been transmitted to a PDP-9 digital computer. The data consisted of the following items: time-of-flight measurements on the event trigger and each of the four detector telescopes, pulse height in each of the shower counters, a set of latches set by the individual detector counters triggered by the event signal, and a similar set of latches triggered by a delayed signal for measurements of accidental coincidences. Approximately 0.5 msec were required to complete this process, of which half was due to the time-to-digital conversion.

After every twelfth event, all scaler data were transmitted to the computer, and a record consisting of the raw event data and the scaler data was written on magnetic tape.

#### G. Comparison with the Most Precise Previous Experiment

This experiment employed the same technique used in the most precise previous experiment.<sup>11</sup> Therefore, it is of value to point out explicitly the major differences between our experiment and that of Sayer *et al.*<sup>11</sup>

(1) The  $T_0$  was derived from a beam-on-target Čerenkov counter rather than from the synchrotron master oscillator, thus avoiding phase drifts of the signal relative to the circulating proton beam.

(2) The position of the detector was varied over a total distance of 73 ft. (The previous experiment had a 15-ft traversal.)

(3) About 10 times the number of events were collected.

(4) A far larger amount of beam time (200 h)

was devoted to the double-chopped injection mode of the synchrotron. This allowed measurements over a larger momentum range and easier analysis of the rf ghost ambiguities.

(5) Although the equipment was similar, the apparatus was entirely new in this experiment.

(6) The previous experiment had but a single collimator, and a serious background was caused by neutrons which scattered into the detector. The double collimator system used in the present experiment eliminated this background almost completely.

(7) The collimation system was moved with the detector to maintain a constant beam size through the detector and thereby gave a position-independent detection efficiency. The previous experiment had a fixed collimator and a  $K_L^0$  detection efficiency that varied with position.

(8) The detector used in Ref. 11 had fourfold symmetry transverse to the beam axis. This was abandoned in favor of an asymmetric geometry for the reason given in Sec. III E.

(9) Lead-Lucite shower counters were included in each of the four sections of the detector.

(10) Experimental backgrounds were measured by filling the primary collimator with mercury, thereby stopping the direct beam. In the previous experiment, the backgrounds were measured by raising a pile of lead bricks into the neutral beam. This in itself could have caused an excessive change in the background.

(11) A spill correlator was used in this experiment to reduce errors in the  $K_L^0$  flux normalization.

(12) For each event, time of flight, some pulse heights, and a set of latches containing the event trigger pattern were recorded on magnetic tape. A similar set of latches with a delayed gate was used as a continuous monitor of accidental triggers. This recording of individual events permitted different selection criteria to be applied to the data in the analysis.

### III. DATA ANALYSIS

#### A. Introduction

All of the data taken were analyzed for the mean-lifetime measurement except for those runs in which there was an obvious malfunction of the apparatus or a mistake in procedure. The experiment was designed so that there are many cross checks in the data set. By making a large number of measurements with high redundancy we hoped to show that resultant measured mean lifetime is not dependent on any single category of detected events. As an example, the responses of the kaon detector may be divided into several different categories, denoted "event types." Each of the event-type rates provides a separate measurement of the kaon-decay rate, and each type may be analyzed independently, giving several results. Since each event type is sensitive to the experimental backgrounds in different ways (the backgrounds from cosmic rays and beam-related particles have strong directionality), the consistency of the various measurements is a check for systematic biases.

The data were analyzed in three stages. In the first stage, the data runs were treated individually. The data were corrected for the TOF calibrations and binned in TOF bins according to their event types and spill-correlator readings. The cosmic-ray and beam-related backgrounds were subtracted. The binned data were normalized, taking into account the corrections to the normalization due to dead times, solid angle changes, etc. In the second stage of the analysis, the data sets from the individual runs at a given detector position were combined. These data sets were checked to determine that the measurements at a given position were consistent within statistical uncertainties. The combined data sets were then subjected to a least-squares fit to determine the mean lifetime of the  $K_L^0$ .

#### B. Analysis of the Individual Runs

##### 1. Event Types

Each detected event was binned by event type. The event types were determined by the pattern of counters which fired during the event. The fast logic system required that both inner counters of two telescopes responded. In addition, the shower counters or counters in other telescopes may have responded. The events were divided into categories: The first six categories contained events where two and only two of the scintillation-counter telescopes responded. These were labeled *AB*, *AC*, *AD*, *BC*, *BD*, and *CD* according to the telescope coincidence pattern (see Fig. 3 for the tele-

scope notation). The seventh category contained events which fired more than two telescopes. The eighth and ninth categories were used for events lacking a  $T_0$  pulse and events where a veto latch bit was set. Table III shows the relative abundance of the various event types for a typical run at the 400-in. position compared with expected (Monte Carlo) values and values for a completely random coincidence pattern. The data shown have no background subtractions, but the backgrounds were quite small for this run. The agreement is satisfactory.

About 2.5% of the events have one or more of the veto latch bits set, whereas one would expect no events in this category since an event pulse should not have occurred if a veto counter fired. These spurious events may be due to differences in timing between the normal kaon detector logic and the readout latch. The rate is too high to be due to accidental counts in the vetoes; it is therefore uncertain whether or not these events should be included in the data set. This matter was solved by fitting for the mean lifetime both with and without using the vetoed events, and showing that the mean lifetime did not change appreciably.

##### 2. Time-of-Flight Binning

The TOF spectrum was condensed from about 200 into 30 bins. The lower time limit was determined by TOF resolution, and the upper time limit was chosen to avoid instrumental cutoffs. For the different positions of the kaon detector and different injection periods, these criteria determined different momentum ranges (see Table II). The conversion from TOF channel to nanoseconds was determined by the measurements of  $A_1$  (described in Sec. II E). The TOF channel corresponding to an infinite-momentum kaon ( $A_0$ ) was measured using converted gamma-ray pairs. The effect of an error in  $A_0$  is a slight mislabeling of the kaon momentum. The measured  $A_0$  was corrected by two factors, the first due to the fact that two different methods were used for  $\gamma$ -ray conversion and the second due to differences in the detector irradiation patterns between  $\gamma$  rays and kaons of various momentum.

These factors result from the displacement of the first moment of the spatial distribution of particles hitting the detector. The irradiation of the detector by  $\gamma$ -ray pairs is stronger at its downstream end, and the irradiation pattern changes if the pairs are produced in different ways. Also, the TOF is determined by the later of the two signals to arrive at the detector logic. This means that the timing is determined by the particle which hits furthest *upstream* in the detector, since the propagation of its signal through the scintillation

TABLE III. Relative frequency of kaon detector responses.

Event type	Percent without shower counter trigger	Percent with shower counter trigger	Renormalized 2 telescope	Total percent predicted by Monte Carlo program	Percent predicted for completely random response
<i>AB</i>	35.8	1.3	39.3	41.1	22.3
<i>AC</i>	12.3	0.4	13.3	13.9	18.8
<i>AD</i>	8.1	0.3	8.8	8.6	16.1
<i>BC</i>	8.7	0.2	9.4	8.7	16.6
<i>BD</i>	6.0	0.2	6.5	5.3	14.2
<i>CD</i>	20.5	1.0	22.7	22.4	12.0
3 and 4 telescope	1.9	0.1	...	...	...
Reset	0.7	0.0	...	...	...
Vetoed	2.4	0.1	...	...	...
Sum	96.4	3.6	100.0	100.0	100.0

plastic is slower than its velocity before impact.

The first additive corrections to the measured  $A_0$  values are required because of the two methods used for converting  $\gamma$  rays. The method used when the detector and collimator carts were close together was to close a  $\frac{3}{8}$ -in.-thick brass valve at the downstream end of the primary collimator which acted as a converter. The collimator sweeping magnet current was reduced and the front veto counter of the detector was disconnected. The second method of converting  $\gamma$  rays consisted in inserting a  $\frac{1}{8}$ -in.-thick lead sheet in the beam 3 ft in front of the active volume of the detector. This method was used when the collimator cart and the detector cart were separated by considerable distance. In general, the lead sheet was used for run types 6, 7, and 8 of Table II. Each method gave results consistent to 0.15 nsec for all runs, but the two methods differed by 0.75 nsec.

The discrepancy was measured by using the TOF peak of the GAMMA monitor as a reference. (See Secs. II D, II E.) An 0.75-nsec correction was applied to the  $\gamma$  peaks resulting from the brass converter in order to make all runs consistent.

The second additive correction to the measured  $A_0$  values is necessary because the kaon decay products and the  $\gamma$ -ray pairs irradiated the detector differently. Also, the decay volume for high-momentum kaons will tend to be farther upstream than that for low-momentum kaons due to the more pronounced forward peaking of decay products from higher-momentum particles. This effect is counteracted in the measured TOF by the lower velocity of the decay products of the low-momentum kaons. Further, the velocity of signal propagation in the scintillator [measured in our detector to be  $(0.50 \pm 0.05)$  times the velocity of light] differs, in general, from the decay-product velocities. A Monte Carlo program was used to analyze these effects.

We found the shift in  $A_0$  timing as a function of momentum to be 0.1 nsec over our range. It is small because of a tendency of various effects to cancel. The timing difference between kaons and  $\gamma$  rays was less well-defined because of uncertainties in the pair distributions in the detector. From the experimental data, however, we were able to determine the direction of the effect and an upper limit to its magnitude. We assigned a 100% uncertainty to the correction. The two corrections together amount to  $0.03 \pm 0.03$  nsec in  $\tau$ .

### 3. Normalization

The normalization factor for an individual run was composed of five multiplicative terms: (1) the number of monitor counts, (2) the solid angle subtended by the detector, (3) the efficiency for obtaining a valid time of flight, (4) a corrective factor for the dead time caused by the veto counters, and (5) the detector efficiency. We emphasize that it is unnecessary to know the *absolute*  $K_L^0$  flux, the momentum spectrum, or the absolute efficiency, i.e.,  $N_0(P)$  and  $\epsilon(D, P)$  in Eq. (2). Relative values are sufficient. In the ratio  $N/N_0$ , these factors cancel when comparing the detected rates at different values of  $D$ , provided that  $\epsilon$  is independent of  $D$ .

*Monitors.* Both the BOT and VM monitors were used to monitor the number of protons striking the production target. The ratio between them showed a systematic variation of about 30% as a function of the proton energy. Averaged over the entire beam spill period, they showed run-to-run discrepancies of a few percent. Further increase in consistency was achieved by analyzing separately the data in each correlator channel (see Sec. II D). Remaining discrepancies were of order 1% and uncorrelated with the detector position. The lifetime analysis was performed independently for each of

the monitors with good agreement.

*Solid Angle.* The effective solid angle of the detector was calculated with the Monte Carlo program. The following factors were taken into account: (1) the finite size of the production target, (2) attenuation of the proton beam through the target, (3) collimator geometry, and (4) some transmission through the edges of the collimator. Solid angles for each run type are given in Table II.

*TOF Efficiency.* Only those events which have a valid TOF measurement can be analyzed, so we must correct for inefficiencies. Further, the efficiency is different for background triggers,  $B$ , and real events,  $E_L$ . It is also a function of beam rate and spill conditions. The number of "reset" counts,  $R$ , for which no TOF measurement exists, is

$$R = (1 - \epsilon_L)E_L + (1 - \epsilon_B)B, \quad (3)$$

where  $\epsilon_B$  is the TOF efficiency for the background, and  $\epsilon_L$  for the legitimate events. It is not possible to determine both efficiencies in a given run. Further, background runs are not a good separate measure of  $\epsilon_B$  since its value is subject to large systematic variations between runs. However,  $\epsilon_L$  (measured in runs with very low background) is a well-defined and almost linear function of the beam rate  $b$ . (Consult the thesis in Ref. 1 for details.) Using this function and Eq. (3), we were able to determine both  $\epsilon_L$  and  $\epsilon_B$ . The error in this procedure is small and leads to a negligible uncertainty in  $\tau$ .

*Veto Dead Time.* A correction was necessary for dead time in the veto counters. This factor tended to be larger when the detector was close to the synchrotron target, which may have been due to radiation diffusing out of the synchrotron shield wall to trigger the veto counters. The dead-time correction was monitored continuously during all runs and ranged from 0.2% to 0.6% of the live time.

TABLE IV. Cosmic-ray background by event type.

Event type	Percentage of CR background
$AB$	18.3
$AC$	37.4
$AD$	12.8
$BC$	7.4
$BD$	5.2
$CD$	5.7
3C and 4C	1.6
Reset	...
Vetoed	4.5
Shower counter trigger <sup>a</sup>	6.9

<sup>a</sup> This category includes all of the event types in the fourth column of Table III.

*Detector Efficiency.* It is impossible to measure the detector's efficiency without a set of "tagged"  $K_L^0$  mesons. The Monte Carlo program was used to compute the efficiency, particularly its position dependence, as a function of kaon momentum. The resultant efficiency was independent of the position of the detector within errors small compared to the statistical uncertainties in the measured rates. Thus, in Eq. (2) we find that  $\epsilon(D, P) = \epsilon(P)$  is independent of  $D$  and can be absorbed into  $N_0(P)$ . In the separate calculation of the absolute production spectrum, the computed values for  $\epsilon(P)$  must be used.

#### 4. Backgrounds - Cosmic-Ray and Beam-Related

Cosmic-ray (CR) background rates were measured in short runs with the logic system gated so that no beam contamination would occur. These runs were taken during the two-hour period required to move and align the collimator and detector carts. Due to the very low rate of cosmic-ray triggers, these runs had poor statistics, and a detailed analysis by event type was not possible. Only the total rate was recorded. To obtain more detailed information on the CR events, long runs were taken at four times throughout the experiment. These runs were put onto magnetic tape and processed like the regular data. The CR-event-type pattern is consistent in each of these runs and the average values are shown in Table IV. Note the considerable difference in event-type ratios from the kaon decays shown in Table III. These average values of the CR-event-type ratios were used for the subtraction of CR background from all of the data runs, but the CR rate for the subtraction from an individual run was determined using the rate from the short CR run taken at the time of that data run.

The CR veto counters eliminated more than 99.8% of the possible CR events. The CR background is due to the remaining inefficiency, which, though small, amounted to half the events when the kaon detector was farthest from the production target. There was a definite suppression of the CR-event rate as the detector was moved far upstream and came into the "shadow" of the synchrotron shield wall. There was one instance of an anomalously high CR event rate, which was traced to a malfunction in a CR veto counter, but in general the CR rates were in statistical agreement at a given detector position.

Beam-related backgrounds (BRBG) were measured by running under normal conditions except that the primary collimator was filled with mercury. These runs, called "plug-shut" runs, were

taken after each data run for a length of time sufficient to equalize the statistical uncertainty in the measured rate with that of the data ("plug-open") runs. The BRBG rate was obtained from the plug-shut runs after a subtraction of the CR background. The BRBG rate (normalized to a beam monitor) was roughly constant throughout the data set at about 0.2% of the detected kaon flux at the 400-in. detector position. With the exception of two runs, the BRBG TOF spectrum was shown to be flat, with acceptable  $\chi^2$  probabilities for fits to a flat spectrum. The exceptions were assumed to be contaminated by beam leakage through the plug. They were consistent with the general BRBG rate, and the best-fit constant value was used.

The subtraction of the background to obtain the number of legitimate kaon decays will be given in terms of the following symbols:

$M_o$  ( $M_s$ ): total monitor counts, plug open (shut)

$C_o$  ( $C_s$ ): total number of clock counts, plug open (shut)

$f$ : CR trigger rate per clock pulse

$r_b$ : BRBG rate per monitor count

$E_L$ : number of legitimate kaons

$E_B$ : beam-related background

$E_{CR}$ : cosmic-ray triggers

$\epsilon_L$  ( $\epsilon_B$ ): TOF efficiency for  $E_L$  ( $E_B$  and  $E_{CR}$ ).

The total number of valid events detected in a given plug-open run is

$$\begin{aligned} E_o &= \epsilon_L E_L + \epsilon_B (E_B + E_{CR}) \\ &= \epsilon_L E_L + \epsilon_B (r_b M_o + f C_o). \end{aligned} \quad (4)$$

In a plug-shut run, we measure

$$E_s = E_B + E_{CR} = r_b M_s + f C_s, \quad (5)$$

irrespective of whether there is a valid TOF. Solving for  $E_L$ , we obtain

$$\begin{aligned} E_L &= (\epsilon_B / \epsilon_L) \left( \frac{E_o}{\epsilon_B} - r_b M_o - \frac{(E_s - r_b M_s) C_o}{C_s} \right) \\ &= (\epsilon_B / \epsilon_L) \left( \frac{E_o}{\epsilon_B} - \frac{E_s C_o}{C_s} - r_b M_o (1 - b_s / b_o) \right) \\ &= E_o / \epsilon_L - B \epsilon_B / \epsilon_L, \end{aligned} \quad (6)$$

where  $b_i = M_i / C_i$  is the "beam rate", the number of monitor counts per unit time, and  $B$ , defined by this equation, denotes the total background. Because the background is uniform over the TOF spectrum, a fraction  $w_i / W$  of  $B$  was subtracted from an individual momentum bin ( $w_i$  is the width of the  $i$ th TOF bin, and  $W$  is the width of the whole spectrum). The quantities  $E_o$ ,  $E_s$ ,  $R$ ,  $C_o$ ,  $C_s$ ,  $M_o$ ,  $b_s$ , and  $b_o$  were measured directly. The TOF efficiencies,  $\epsilon_L$  and  $\epsilon_B$ , were discussed in the previous section. The BRBG factor  $r_b$  was computed for each plug-shut run by subtracting the computed number of CR counts from the total plug-shut events, i.e.,  $r_b = (E_s - f C_s) / M_s$ , where  $f$  denotes the measured CR rate at the time of the run. The computed  $r_b$  are shown in Fig. 6, where they are plotted as a function of run number and type. The background rate was constant, within statistical fluctuations, for each run type. An average value of  $r_b$  was used for all runs. The possible deviation of type 7 from this does not affect our final results.

Although  $r_b$  may be uncertain by as much as a factor of 2, it has only a slight influence on  $E_L$  in

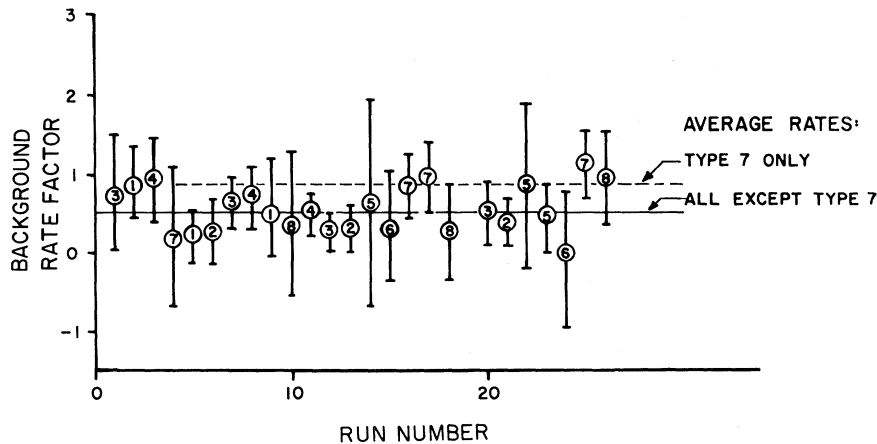


FIG. 6. Computed BRBG rate factor,  $r_b$ , versus run number. The numbers inside the circles on this plot refer to the run type as specified in Table II. The average values of  $r_b$  used in the analysis are shown by the horizontal lines.

Eq. (6) because  $b_s/b_o \approx 1$ , i.e., the beam rate was fairly constant.

### C. Selection of the Final Data Set

In choosing a final data set, two cuts were made. In the first cut, the data in correlator channels 1 and 2 were eliminated. In the second cut, the data for run types 7 and 8 were discarded.

The data taken in correlator channels 1 and 2 were strongly influenced by changes in the operation of the synchrotron. These correlator channels cover bands at the early and late ends of the spill totaling 3.8 msec (see Table I). The beam spill during these periods was erratic, causing large fluctuations in TOF efficiency. Also, during periods of "double-chopped" injection, the spill was shortened, giving relatively less beam in these channels. Considering only runs with low CR contamination, the TOF efficiency ranges from 92% to 99% in correlator channel 1, while it ranges from 97.5% to 99.6% in correlator channel 4 for the same data set.

The data in correlator channels 1 and 2 constituted about 18% of the total. It was originally taken to estimate the effects of variations in proton energy and rate within the beam spill. After consideration of the comparatively limited statistical weight of the data and the uncertainties in the estimation of the TOF efficiency, it was apparent that these data would not be useful as a tool to probe systematic effects in the analysis of the remaining data. They are not included in the final fit for the lifetime.

In the analysis of the data for run types 7 and 8 (the 50-ft and 73-ft detector positions; see Table II) it was found that the data for these run types were different in character from those of other run types. The ratios of the various event types for these runs showed an anomalously high rate of events where two adjacent telescopes had fired (types *AC*, *AD*, *BC*, and *BD* in Table III) compared with the number of events where opposite telescopes fired (*AB* and *CD* event types). The "adjacent" events had almost twice their normal rates.

The source of these triggers may have been neutron flux from the primary collimator walls. When the detector and collimator carts were separated, the detector was no longer completely in the "shadow" of the secondary collimator. The dominance of the adjacent triggers may then be explained by noting that a neutron striking the detector near a corner between two telescopes has a much higher probability of triggering these two telescopes than any neutron has of triggering an "opposite" event.

The collimator and detector carts were separated for run types 6, 7, and 8. The data of type

6 did not show abnormal event-type ratios. Compared with types 7 and 8, the kaon rate in type 6 is much higher. Also the detector is better shielded in the type-6 positions. Therefore type 6 was retained in the data set, whereas types 7 and 8 were discarded.

Although we choose to reject these data due to the possibility of background contamination, we have performed the analysis with them included. The result differs negligibly from our final value. Our retention of type 6 is justified by its consistency with type 4, as demonstrated in Sec. III D.

### D. The Internal Consistency of the Data Set

Many different fits were made to the data, applying different cuts, normalization factors, and so on. Each time a set of data runs was selected for analysis, the binned momentum spectrum for each run was compared with other runs of the same type using a  $\chi^2$  test. A typical result of this comparison of similar runs is shown in Fig. 7. In addition to plotting the total  $\chi^2$ , the contributions to  $\chi^2$  were examined for normalization shifts and single points with abnormally high discrepancies. In the final data set there were no  $\chi^2$  values higher than 50 for 30 degrees of freedom, and the  $\chi^2$  distributions were generally acceptable. It should be noted that this comparison procedure will not detect many classes of systematic errors, but it will overemphasize discrepancies between two data sets with different background subtractions, since subtractions from the channels are correlated.

In addition to comparing the spectra, the consistency among some of the run types can be checked using the lifetime fitting program. The fitting program was used to compare run types 1 and 5, both of which are taken at the 0-ft position, and to compare types 4 and 6, both of which are taken at the

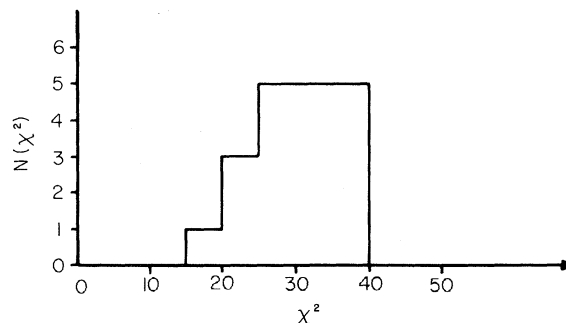


FIG. 7.  $\chi^2$  distribution for a typical spectrum comparison of similar runs. Since there are 30 bins in each spectrum, it is expected that the  $\chi^2$  histogram should peak near 30, and that it should have a FWHM of 11. The lack of large  $\chi^2$  shows that the data are internally consistent.

25-ft position. Type-1 data are taken with single-chopped injection, while type-5 data were taken with double-chopped beam. Thus types 1 and 5 should have the same rate, but type 1 will be "folded over" (cf. Fig. 2) whereas type 5 will not. A  $\chi^2$  comparison of these two spectra (with a fixed kaon lifetime) tests the consistency of the two spectra and checks the program. The  $\chi^2$  probabilities for these fits were always acceptable.

#### E. The Monte Carlo Program

A Monte Carlo program was written before the construction of the experiment to aid in its design and to study the response of the kaon detector. In simulating the kaon decays, the branching ratios, kinematics, and known energy spectra for the decays were used. A simulation of the physical and geometrical properties of the detector was generated. The behavior of the various decay products and their interaction with the detector was programmed by including multiple scattering, pion decay, and energy loss by ionization.

The logic of the electronic triggering was also simulated to enable comparison with measured event-type ratios. A symmetric detector provides only one experimentally measurable quantity which can be compared to a Monte Carlo simulation: the opposite-adjacent counter event ratio. Four similar quantities are fixed by the symmetry. The asymmetric detector used in this experiment provides five different ratios among the six types of event trigger patterns. These are, at least in part, dependent on the kinematics of  $K$  decay, and provide a basis for comparison with Monte Carlo calculations. The measurements and calculations agreed well for the asymmetric detector, indicating that both the Monte Carlo simulation and the detector properties are understood.

As mentioned in Sec. II G, the experiment was designed to make the efficiency,  $\epsilon(D, P)$  in Eq. (2), independent of the distance,  $D$ . The Monte Carlo results confirm this. For the lifetime calculation, described in the next section,  $\epsilon(P)$  was absorbed into  $N_0(P)$ . However, values of  $\epsilon(P)$  computed by the Monte Carlo program were used to extract the absolute production spectrum from the fitting parameters,  $N_i$ .

#### F. The Lifetime Fitting Program

This program is used to determine the best "least-squares" fit for the  $K_L^0$  mean lifetime. In addition to fitting for  $\tau$ , the program simultaneously fits for a set of nine parameters ( $N_i$ ) which describe the kaon production spectrum at the synchrotron target after multiplication by the efficiency for detecting a kaon that passes through the ap-

paratus. The parameters  $N_i$  form a piecewise linear fit to the kaon momentum spectrum, and  $N_0(P)$  in Eq. 2 is determined from this fit by calculating the area in a momentum bin of width  $\Delta p$  and mean momentum  $P$ . Thus, both  $\tau$  and  $N_0(P)$  are unknowns in Eq. (2) to be determined by fitting, but  $N_0(P)$  is approximated by the  $N_i$ . This procedure of linearly interpolating between discrete points of the kaon momentum spectrum was tested and found to introduce no systematic errors in the results.

Given a first approximation to the momentum spectrum, we fit the data set for the best value of  $\tau$ . The process is iterative, with  $\tau$  and the  $N_i$  being varied until a minimum is obtained for  $\chi^2$ . The explicit form of  $\chi^2$  is

$$\chi^2 = \sum_{j=1}^6 \sum_{k=1}^{30} W_{jk} (K_{jk} - F_{jk})^2 / \Delta_{jk}^2, \quad (7)$$

where the  $j$  sum refers to the six run types (Table II) and the  $k$  sum refers to the 30 momentum bins. The quantity  $w_{jk}$  is either zero or unity, depending on whether a particular data point is included in the fit.  $K_{jk}$  is the normalized detected kaon rate and  $\Delta_{jk}$  is its uncertainty.  $F_{jk}$  is the number of particles calculated by Eq. (2) to be in the momentum range corresponding to  $K_{jk}$ , including the fold-over or ghost spectrum. Each  $F_{jk}$  is a function of the production spectrum parameters,  $N_i$ , and the lifetime,  $\tau$ .

#### G. Statistical Errors

The statistical error associated with the fitted value of  $\tau$  was found in the fitting process. The  $\chi^2$  fitting program required a statistical uncertainty for each input data point [ $\Delta_{jk}$  in Eq. (7)]. These came mainly from  $E_o$  and  $E_s$  in Eq. (6), i.e., from the measured event rates. The uncertainty in  $\tau$  was determined numerically by varying  $\tau$  until  $\chi^2$  increased by one unit over its minimum value.

#### H. Systematic Errors

Systematic errors in this experiment may be divided into three categories: (1) uncertainties in fitting derived quantities ( $e_L$  and  $r_b$ ), (2) uncertainties arising from systematic variation in measured parameters (monitor drifts, efficiency changes, calibration changes, etc.), and (3) possible errors due to approximations in the analysis.

As described in Sec. III B, we used approximations for the TOF efficiency and the background rates. The sensitivity of  $\tau$  to these approximations was determined by changing the approximation, and fitting the same data set again. Using this method, we determined the possible systematic uncertainties shown in Table V. The estimated uncertainties in the parameters represent conservative judgments.

TABLE V. Contributions of systematic errors to the error in  $\tau$ .

Error type	Relative change in $\tau$	Estimated uncertainty	Contribution to fitted $\tau$ (nsec)
$A_1$	0.26 nsec/percent	0.4%	0.10
$A_0$	0.05 nsec/nsec	0.5 nsec	0.03
$\epsilon_L$	0.02 nsec/percent	0.5%	0.01
$r_b$	0.0012 nsec/percent	30%	0.04
ABC	0.4 nsec/percent	0.1%	0.04

Similar procedures were used for the TOF calibrations,  $A_0$  and  $A_1$ . Run-to-run shifts in  $A_0$  were probably considerably less than the value of 0.5 nsec listed, but the over-all uncertainties in the  $\gamma$ -pair calibration procedure lead us to select this figure. The estimated 0.4% uncertainty in  $A_1$  represents observed changes during the course of the experiment.

Alternate bucket contamination (ABC) was described in Sec. II E. It was measured continuously and subtracted directly from the TOF spectra for individual runs. Since it was generally at the noise level of the measuring system, it was assigned a 100% uncertainty. Its magnitude was determined by fitting for a lifetime both with and without the correction.

Systematic errors may arise in combining the individual runs. For example, the normalization may have changed over a period of time, and the runs may indicate different rates. The use of spectrum comparison tests, as described in Sec. III D, has shown that the final data set is self-consistent. Any unobserved residual effects should be accounted for by the quoted statistical uncertainty.

Tests were made for systematic effects due to approximations made in the analysis. A data set was simulated using Monte Carlo techniques. This set had a known mean lifetime, and the data were made to resemble a genuine data set, including simulated statistical fluctuations. The simulated data were fitted using the same analysis program as for the real data. For three independent simulated data sets, the analysis program gave a fitted mean lifetime within one standard deviation of the known value. Since the properties of the simulated data set (the number of total events, the momentum spectrum, and so on) were chosen to correspond closely to the properties of the real data set, the fits to simulated data gave an excellent estimate of the expected statistical uncertainty and the relative importance of systematic effects related to approximations used in the real analysis.

We have assumed no correlation among the un-

certainties and have added them in quadrature to obtain an over-all systematic uncertainty of  $\pm 0.12$  nsec.

## IV. RESULTS

### A. $K_L^0$ Lifetime

Using our best data, we have determined

$$\tau = (5.154 \pm 0.044) \times 10^{-8} \text{ sec}$$

for the mean lifetime of the  $K_L^0$  meson. The least-squares fit gave  $\chi^2 = 114$  for 107 degrees of freedom (DF). The uncertainty is dominated by a statistical uncertainty of 0.42 nsec, with a contribution of 0.12 nsec from systematic effects added in quadrature. The final data set consisted of 449 234 detected events. Of these 13 774 were subtracted as background.

The fit to the data is displayed in Fig. 8. The natural logarithm of the attenuation,  $N/N_0$ , is plotted versus  $MD/P\tau$ , the number of mean lives. Ghosts are subtracted from the data in the figure to avoid confusion. The data taken at the two positions farthest from the source were not used for reasons discussed in Sec. III C. They are included in Fig. 8 to show that the exponential decrease continues beyond the limits of what we consider good data.

In the remainder of this section we present fits to various subsets of the data.

#### 1. Fit to Different Correlator Channels

The final result is the weighted average of two independent fits of the data from correlator channels 3 and 4 using the VM monitor for normalization:

$$\tau = 51.12 \pm 0.89 \text{ nsec}, \quad \chi^2/\text{DF} = 119/107;$$

$$\tau = 51.61 \pm 0.47 \text{ nsec}, \quad \chi^2/\text{DF} = 115/107.$$

These two data sets we denote by VM3 and VM4, respectively.

#### 2. Fit with Different Normalization

$$\tau = 51.61 \pm 0.96 \text{ nsec}, \quad \chi^2/\text{DF} = 125/107;$$

$$\tau = 51.46 \pm 0.48 \text{ nsec}, \quad \chi^2/\text{DF} = 113/107.$$

These data were normalized to the BOT monitor but are otherwise similar to VM3 and VM4.

#### 3. Fit Including "Vetoed" Events

Adding the events in which a veto counter latch bit was set (see Sec. III B 1) gave for the VM4 set

$$\tau = 51.36 \pm 0.46 \text{ nsec}, \quad \chi^2/\text{DF} = 120/107.$$

The "vetoed" events were not included in the final data set.

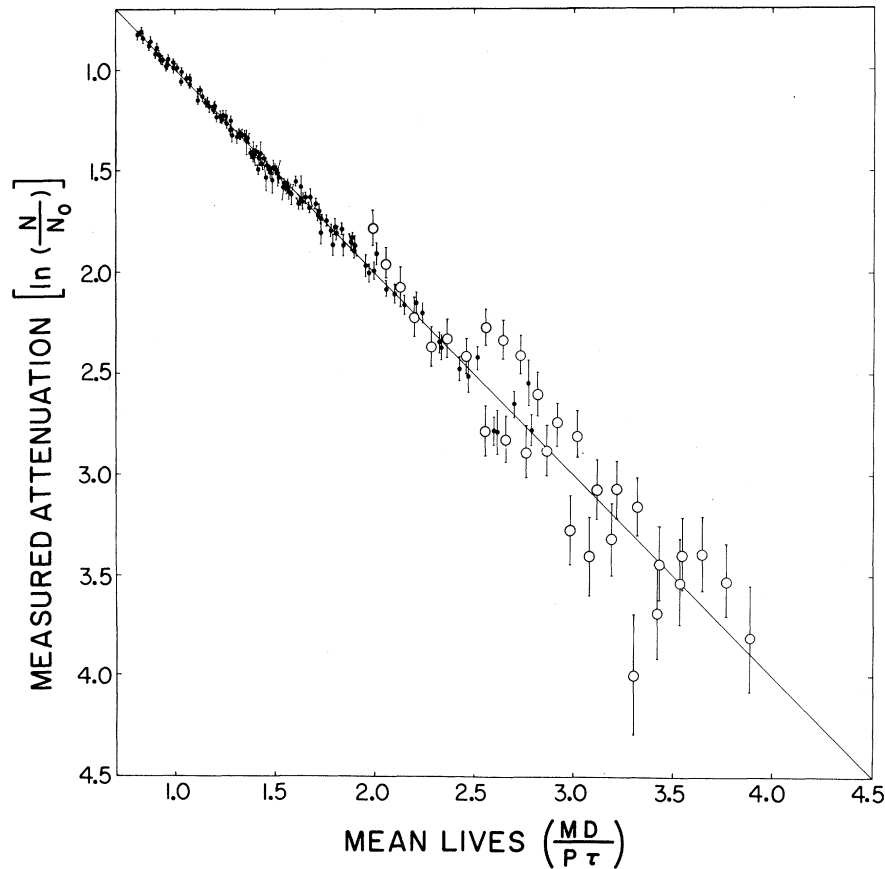


FIG. 8. The logarithm of the observed relative intensity of  $K_L^0$  mesons as a function of the proper time in units of the fitted mean lifetime. The solid curve is the exponential fit to the data. The open circles represent data from run types 7 and 8 which were not used in the final analysis. The solid circles represent the data from run types 1-6 used in the fit.

#### 4. Fit Deleting Events with Shower Counter Triggers

If the events in which a shower counter fired (see Table III) are deleted from the VM4 data set, we obtain

$$\tau = 51.69 \pm 0.49 \text{ nsec}, \quad \chi^2/\text{DF} = 112/107.$$

The change of 0.07 nsec is small compared with the estimated statistical uncertainty, and events in which a shower counter fired were included in the final data set.

#### 5. Fit by Event Types

The events in set VM4 were divided into two categories. The opposite category included types  $AB$  and  $CD$  (cf. Table IV), while the adjacent category included types  $AC$ ,  $AD$ ,  $BC$ , and  $BD$ .

For the opposite and adjacent types we get, respectively,

$$\tau = 51.79 \pm 0.63 \text{ nsec}, \quad \chi^2/\text{DF} = 118/107;$$

$$\tau = 51.30 \pm 0.84 \text{ nsec}, \quad \chi^2/\text{DF} = 93.5/107.$$

#### 6. Chronological Cuts

The VM4 data set was divided into two halves, each corresponding to two weeks in the running. In order, the "early" and "late" periods give

$$\tau = 52.29 \pm 0.81 \text{ nsec}, \quad \chi^2/\text{DF} = 83/90;$$

$$\tau = 51.07 \pm 0.59 \text{ nsec}, \quad \chi^2/\text{DF} = 115/90.$$

#### 7. Momentum Cuts

Four equal momentum bands were set from 200 to 400 MeV/c, and the bands were fitted separately. It is not possible to make completely independent measurements in this way, since all of the momentum bins in data type 5 must be included so that the "ghosts" can be evaluated (see Sec. II E). The four momentum ranges gave

$\tau$ (nsec)	$\chi^2/\text{DF}$	$P$ (MeV/c)
$52.29 \pm 0.91$	69/43	200-250
$51.85 \pm 1.17$	83/60	250-300
$50.23 \pm 1.43$	71/56	300-350
$50.69 \pm 1.01$	56/60	350-400

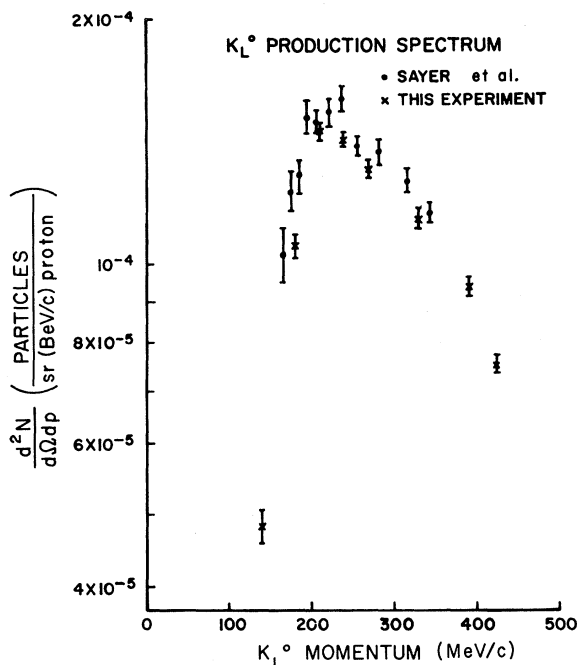


FIG. 9. The number of  $K_L^0$  produced per unit solid angle, per GeV/c per incident proton (3 GeV) on a 1.5-in. platinum target obtained in this experiment, compared with results of Sayer *et al.* [Phys. Rev. **169**, 1045 (1968)].

The apparent systematic trend with momentum is not significant. Such a result can be expected to occur by chance about 20% of the time.

The comparisons above indicate a high degree of internal consistency in our data. They suggest the absence of large systematic errors which are dependent on time in spill, beam rate, normalization, momentum cuts, calibration drifts, and certain types of backgrounds.

We have computed a weighted average of our result with the previously measured values of  $\tau$ .<sup>10-16</sup> We find

$$\tau = (5.152 \pm 0.042) \times 10^{-8} \text{ sec}$$

as a new world average. The best previous measurement<sup>11</sup> gave  $\tau = 51.5 \pm 1.4$  nsec, in excellent agreement with our result, but the previous constrained fit value published by the Particle Data Group<sup>6</sup> ( $53.8 \pm 1.9$  nsec) differs by 4.3%. A new calculation of the constrained fit has been performed<sup>18</sup> including our new result. It gives  $\tau = (5.172 \pm 0.043) \times 10^{-8}$  sec.

#### B. $K_L^0$ Production Spectrum

We have divided the fitted spectrum parameters,  $N_i$ , by the appropriate values of  $\epsilon(P)$ , the detection efficiency as determined by the Monte Carlo calculation. The results are plotted in Fig. 9 in terms

of the number of particles produced in a  $1\frac{1}{2}$ -in. platinum target. There is a systematic difference of about 10% between our results and those of Sayer *et al.*<sup>11</sup> Two possible effects could contribute to this difference. Due to the selection of data in correlator channels 3 and 4, the present experiment may sample a higher average proton energy than the previous experiment. There are, also, calibration uncertainties in comparing monitor rates at widely separated times.

#### C. The Velocity of Light

The use of the GAMMA monitor to calibrate the time-of-flight system gives us an opportunity to measure the velocity of high-energy gamma rays. Corresponding displacements in distance and TOF are measured. If we assume that most of the  $\gamma$  rays in our beam originate from  $\pi^0$  mesons which are produced and decay in the target, we can expect the energy spectrum to peak in the neighborhood of 70–100 MeV. Dispersive effects have been sought for photons up to 6 GeV and found to be absent.<sup>19</sup> Therefore, we can safely adopt the conventional value of the velocity of light and use our measurement as a check on the accuracy of the TOF system. We find

$$c = (2.998 \pm 0.033) \times 10^8 \text{ m/sec},$$

in good agreement with the conventional value. This gives strong evidence supporting the accuracy of our  $A_0$  calibrations (see Sec. II E).

#### V. DISCUSSION

Using our present result, the Particle Data Group has recalculated the value of the branching ratio,  $T_3$ , as given in Eq. (1).<sup>18</sup> The value found is

$$T_3 = 1.184 \pm 0.028,$$

as compared with the previous value of  $1.22 \pm 0.05$ . We see that the uncertainty has been reduced considerably, and that the deviation from the expected value of 1.000 is more than six standard deviations.

We can interpret this result in terms of  $\Delta I = \frac{3}{2}$  transitions under the following assumptions: (a) There is no  $I=3$  contribution to the final state.<sup>3</sup> (b)  $CP$  noninvariance is small – of the order observed in  $K_L^0$  decay into two pions. We express the results in terms of the ratio of the reduced matrix elements for  $\Delta I = \frac{3}{2}$  and  $\frac{1}{2}$  transitions to the  $I=1$  final state (as in Ref. 2):

$$R_3 = \frac{\langle \mathbf{1} \| T_{3/2} \| \frac{1}{2} \rangle}{\langle \mathbf{1} \| T_{1/2} \| \frac{1}{2} \rangle}. \quad (9)$$

In this notation,

$$T_3 = \frac{|1 - \frac{1}{2}R_3|^2}{|1 + R_3|^2} \quad (10)$$

and we find that  $R_3 = -0.056 \pm 0.008$ . It is interesting to note that this amplitude ratio is of the same order as that observed in  $K^+$  decay into two pions, the only other well-established example of an  $\Delta I = \frac{3}{2}$  transition.<sup>5</sup> It is reasonable to speculate that these effects arise from electromagnetic corrections to the over-all transition. This explanation, however, would also permit the existence of  $\Delta I = \frac{5}{2}$  transitions, which have been shown to be less than 1%.<sup>3</sup> On the other hand, the current-current picture for weak interactions contains a natural place for  $\Delta I = \frac{3}{2}$  transitions to purely hadronic final states. With this description, one would expect corresponding effects in the hadronic decays of baryons.

No such evidence is found.

One possible source of  $\Delta I = \frac{3}{2}$  terms is the  $\eta$  meson as a virtual intermediate state. This has been discussed by several authors.<sup>20-22</sup> A comparison<sup>23</sup> with the rate for  $K_L \rightarrow 2\gamma$  gives some support to this view.

## VI. ACKNOWLEDGMENTS

We are indebted to Professor M. G. White, Professor W. Wales, and the staff of the Princeton-Pennsylvania Accelerator for their excellent support during all stages of this work. Carl Muehleisen provided technical assistance, Shaw Ling Hsu contributed to the data analysis, and Kyriakos Papodimitriou and Peter Brill helped build the counters.

\*Work supported in part by National Science Foundation under Grants No. GU-1592 and GP-14703 and by the U. S. Atomic Energy Commission under Contract No. AT(30-1)-3651.

†This work is based on a thesis submitted by Kirby G. Vosburgh in partial fulfillment of the requirements for the degree of Doctor of Philosophy at Rutgers University. Present address: Princeton Particle Accelerator, Physics Department, Princeton University, Princeton, N. J. 08540.

‡Present address: Rutherford High Energy Laboratory, Chilton, Didcot, Berkshire, England.

§Present address: Vista Gardens, Apt. 3a, Laurel Road, Nyack, New York.

|| Present address: Physics Department, Virginia Polytechnic Institute, Blacksburg, Virginia 24061.

\*\* Present address: Physics Department, University of Pittsburgh, Pittsburgh, Pennsylvania 15213.

<sup>1</sup>K. G. Vosburgh, T. J. Devlin, R. J. Esterling, B. Goz, D. A. Bryman, and W. E. Cleland, *Phys. Rev. Letters* **26**, 866 (1971); K. G. Vosburgh, Ph.D. thesis, Rutgers University, 1970 (unpublished).

<sup>2</sup>R. H. Dalitz, *Proc. Roy. Soc. (London)* **A69**, 527 (1956).

<sup>3</sup>T. J. Devlin and S. Barshay, *Phys. Rev. Letters* **19**, 881 (1967).

<sup>4</sup>B. Aubert, in *Proceedings of the Topical Conference on Weak Interactions, CERN, 1969* (CERN, Geneva, 1969).

<sup>5</sup>G. Källén, *Elementary Particle Physics* (Addison-Wesley, Reading, Mass., 1964).

<sup>6</sup>Particle Data Group, *Phys. Letters* **33B**, 7 (1970).

<sup>7</sup>G. Trilling, Argonne National Laboratory Report No. ANL-7130, 1965 (unpublished). Updated version: Lawrence Radiation Laboratory Report No. UCRL-16473 (unpublished).

<sup>8</sup>T. J. Devlin, *Phys. Rev. Letters* **20**, 683 (1968); B. G. Kenny, *Phys. Rev.* **175**, 2054 (1968).

<sup>9</sup>T. S. Mast, L. K. Gershwin, M. Alston-Garnjost, R. O. Bangerter, A. Barbaro-Galtieri, J. J. Murray, F. T. Solmitz, and R. D. Tripp, *Phys. Rev.* **183**, 1200 (1969).

<sup>10</sup>T. J. Devlin, J. Solomon, P. Shepard, E. F. Beall, and G. A. Sayer, *Phys. Rev. Letters* **18**, 54 (1967).

<sup>11</sup>G. A. Sayer, E. F. Beall, T. J. Devlin, P. Shepard, and J. Solomon, *Phys. Rev.* **169**, 1045 (1968).

<sup>12</sup>M. Bardou, K. Lande, L. M. Lederman, and W. Chinowsky, *Ann. Phys. (N.Y.)* **5**, 156 (1958).

<sup>13</sup>J. Darmon, A. Rousset, and J. Six, *Phys. Letters* **3**, 57 (1962).

<sup>14</sup>P. Astbury, A. Michelini, C. Verkerk, F. Verkerk, W. Beusch, M. Pepin, and A. M. Pouchon, *Phys. Letters* **18**, 178 (1965).

<sup>15</sup>T. Fujii, J. Jovanovich, F. Turkot, G. T. Zorn, and M. Deutsch, in *Proceedings of the Twelfth International Conference on High Energy Physics, Dubna, 1964*, edited by Ya. A. Smorodinskii (Atomizdat, Moscow, 1966).

<sup>16</sup>J. P. Lowys, B. Aubert, L. M. Chounet, C. Pascaud, and L. Behr, *Phys. Letters* **24B**, 75 (1967).

<sup>17</sup>P. Shepard, T. Devlin, R. Mischke, and J. Solomon, Princeton-Pennsylvania Accelerator Report No. PPAR-10, 1969 (unpublished).

<sup>18</sup>(We are grateful to Dr. A. Barbaro-Galtieri for performing this calculation and giving us the results prior to publication.) Particle Data Group, *Rev. Mod. Phys.* **43**, S1 (1971).

<sup>19</sup>T. Alväger, F. J. M. Farley, J. Kjellman, and I. Wallin, *Phys. Letters* **12**, 260 (1964).

<sup>20</sup>One finds an instructive discussion of this process in R. E. Marshak, Riazuddin, and C. P. Ryan, *Theory of Weak Interactions in Particle Physics* (Wiley-Interscience, New York, 1969).

<sup>21</sup>C. Bouchiat, J. Nuyts, and J. Prentki, *Phys. Letters* **3**, 156 (1963).

<sup>22</sup>Y. S. Kim and S. Oneda, *Phys. Letters* **8**, 83 (1964).

<sup>23</sup>T. J. Devlin, *Phys. Rev. D* **5**, 1674 (1972).